Phosphogluconolactonase as the linchpin of an efficient pentose phosphate pathway

Léa Phégnon[1‡], Julien Pérochon[1‡], Sandrine Uttenweiler-Joseph[1], Edern Cahoreau[1,2], Pierre Millard[1,2] and Fabien Létisse[1,3*]

[1]Toulouse Biotechnology Institute, Université de Toulouse, INSA, UPS, Toulouse, France.

[2]MetaToul-MetaboHUB, National Infrastructure of Metabolomics and Fluxomics, Toulouse, France.

[3]Institut de Pharmacologie et de Biologie Structurale (IPBS), Université de Toulouse, CNRS, Université Toulouse III - Paul Sabatier (UT3), Toulouse, France

***Corresponding author**

Fabien Létisse: fabien.letisse@univ-tlse3.fr

[‡]Co first authors

15 **ABBREVIATIONS:**

16 6PGL : 6-Phosphogluconolactone

17 δ-6PGL : δ-6-phosphogluconolactone

18 GNT: Gluconate

19 6PGNT: 6-phosphogluconate

20 oxPPP: oxidative branch of the pentose-phosphate pathway

21

22

23

ABSTRACT:

The metabolic networks of microorganisms are remarkably robust to genetic and environmental perturbations. This robustness stems from redundancies such as gene duplications, isoenzymes, alternative metabolic pathways, and also from non-enzymatic reactions. In the oxidative branch of the pentose-phosphate pathway (oxPPP), 6-phosphogluconolactone hydrolysis into 6-phosphogluconate is catalysed by 6-phosphogluconolactonase (Pgl) but in the absence of the latter, the oxPPP flux is thought to be maintained by spontaneous hydrolysis. However, in Δ*pgl Escherichia coli*, an extracellular pathway can also contribute to pentose-phosphate synthesis. This raises question as to whether the non-enzymatic reaction can compensate for the absence of 6-phosphogluconolactonase and, ultimately, on the role of 6-phosphogluconolactonase in central metabolism. Our results indicate that in the absence of Pgl, this bypass pathway accounts for the entire flux into the oxPPP, suggesting that non-enzymatic hydrolysis does not compensate for the absence of Pgl and demonstrating that Pgl is critical for an efficiently functioning oxPPP.

INTRODUCTION

Metabolic networks are a set of interconnected chemical reactions, most of which are catalysed by enzymes. The interplay between chemical reactions provides alternative routes for adaptation to genetic or environmental perturbations; the network organisation of metabolic systems thus underpins the metabolic robustness and adaptability of cells. The central metabolism of *Escherichia coli* is a model of metabolic robustness since very few of the associated genes are indispensable for growth on glucose minimal medium[1,2]. Furthermore, *E. coli* knock-out mutants lacking key central metabolic enzymes have similar growth phenotypes[3–7]. This robustness is in part the result of metabolic flux rerouting[6,7] but stems also from local compensatory mechanisms based on redundancy, such as the presence of isozymes and alternative pathways[2–5,7].

Compensatory mechanisms involving non-enzymatic reactions are harder to identify because they cannot be studied by metabolic reconstruction using comparative genomics[8]. These mechanisms are based on specific or non-specific chemical reactions that occur either exclusively non-enzymatically within the metabolic network, or in parallel to existing enzyme functions[9]. The second step in the oxidative branch of the pentose-phosphate pathway (oxPPP), the spontaneous hydrolysis of δ-6-phosphogluconolactone (δ-6PGL) into 6-phosphogluconate (6PGNT) is an archetypal example of a reaction that can occur enzymatically, catalysed by 6-phosphogluconolactonase (Pgl, EC 3.1.1.31), and non-enzymatically, without Pgl activity. However, Pgl's main role, rather than maintaining the flux through the PPP, is thought to be preventing the formation of unwanted side-products by covalent modification with highly reactive 6PGLs (δ (1-5) and γ (1-4))[10–12]. In pioneering studies, Kupor and Fraenkel[13,14] found that absence of the *pgl* gene indeed slowed the growth of *E. coli* on glucose, but more importantly perhaps, they also discovered an alternative pathway bypassing Pgl, involving dephosphorylation and secretion of gluconolactone, spontaneous abiotic hydrolysis in the medium, and re-import of gluconate and phosphorylation[14]. This "Pgl bypass" can therefore provide the same anabolic precursors (NADPH and pentose-phosphates) as the canonical oxPPP.

In *E. coli*, one fifth of glucose uptake is directed towards the oxPPP to provide the required anabolic precursors[6], highlighting the importance of this pathway. In the absence of Pgl, it is thought that this flux is maintained by rapid non-enzymatic hydrolysis of δ-6PGL rather than by the Pgl bypass[7,11,14,15]. However, 6PGLs have a non-negligible lifetime[11], raising the questions whether spontaneous δ-6PGL hydrolysis is fast enough to maintain a high flux through the oxPPP in the absence of Pgl and how the bypass pathway might contribute.

In this study, we used a metabolic flux approach to investigate *E. coli* oxPPP function in the absence of Pgl to (i) reinvestigate the extracellular bypass pathway identified by Kupor and Fraenkel using state-of-the-art methods, (ii) quantify its contribution to oxPPP flux, and (iii) elucidate the metabolic function of Pgl. In the absence of Pgl, we found that virtually all carbon flux through the oxPPP was channelled through the Pgl bypass, and that the contribution of non-enzymatic δ-6PGL hydrolysis was negligible. This in turn suggests that the catalytic function of Pgl is required to maintain high flux through the canonical oxPPP, and that the metabolic role of this enzyme is more substantial than simple house-cleaning duties.

RESULTS

Slow growth in *E. coli* Δ*pgl* is accompanied by gluconate accumulation in the culture medium

We first sought to determine the growth phenotype of an *E. coli* K-12 strain lacking *pgl*, grown on minimal medium with glucose (15 mM) as sole carbon source (Table 1 and supplementary 1 figure 1). In agreement with Kupor and Fraenkel's[14] findings, the Δ*pgl* strain grew much slower than the WT. The rate of acetate production was markedly increased in the Δ*pgl* strain, resulting in a higher acetate yield (0.54 ± 0.03 mol/mol) than in the WT strain (0.31 ± 0.02 mol/mol), as observed previously[7]. In addition to acetate and other metabolites previously detected by ^{1}H NMR[16], significant amounts of gluconate were also detected, but only in the culture medium of the Δ*pgl* strain (Table 1 and supplementary 1 figure 2). Gluconate accumulation represented approximately 2% of the total carbon flux entering the central metabolic pathways of the *Δpgl* strain (Table 1). Note that no 6PGL was detected in the culture supernatant of the *Δpgl* strain (Supplementary 1 figure 2). Complementation of the Δ*pgl* strain with the WT gene restored the growth rate determined for the WT *E. coli*, without any gluconate accumulation (Table 1), demonstrating that reduced growth and gluconate excretion are related to the absence of Pgl.

Gluconate is formed by abiotic degradation of gluconolactone

In the extracellular Pgl bypass proposed by Kupor and Fraenkel[14], gluconolactones are hydrolysed into gluconate abiotically in the culture medium. The obvious explanation for the presence of gluconate in the extracellular medium is therefore that gluconolactones are fully converted into gluconate within the time taken to sample the culture medium and store the samples. To prevent abiotic hydrolysis, the culture medium was sampled by filtration, placed immediately on ice and then analysed by NMR, with the first spectrum recorded approximately 5 min after sample withdrawal. Both isomeric forms of gluconolactone (δ and γ) were detected in equal amounts whereas the gluconate concentration was below the detection limit (Supplementary 1 figure 3). 6PGL was not detected either. Importantly, the total amount of gluconolactones was similar to the amount of gluconate detected in the corresponding

sample obtained with the initial procedure, indicating that rapidly reducing the sample temperature prevents the spontaneous degradation of gluconolactones. To confirm this effect, we measured the rate constants of gluconolactone spontaneous non-enzymatic hydrolysis in fresh minimal medium containing commercial gluconolactone using real-time ^{1}H-NMR (Figure 1). The degradation constants obtained by fitting the gluconolactone concentration–time curves assuming a first-order process[17] were 0.36 ± 0.01 h^{-1} at 7 °C and 2.58 ± 0.02 h^{-1} at 37 °C. At 7 °C therefore, the amount of gluconolactone hydrolysed during 5 min of sample preparation is negligible. Using the same approach, the hydrolysis rate of δ-6PGL was found to be 3.97 ± 0.04 h^{-1} at 37 °C, about 6-7 times higher than at 5°C[11] (Supplementary 1 figure 4) and the same order of magnitude as measured for gluconolactone.

The detection of gluconate in the culture medium in the above experiments is therefore an experimental artefact arising from the hydrolysis of gluconolactones during the sampling process. The Δ*pgl* strain produces gluconolactone (not gluconate) during growth on glucose.

Glucose-derived gluconate is metabolized by canonical gluconate metabolism

Under growth conditions at 37°C, gluconolactones in the culture medium spontaneously hydrolyse to gluconate. However, gluconate remained below the limit of detection when the culture medium was sampled by filtration and rapidly cooled. We therefore hypothesized that the cells consumed gluconate faster than the rate of production by spontaneous hydrolysis. To confirm this, we blocked gluconate utilization by knocking out the two gluconokinases, GntK and IdnK, known to activate gluconate after uptake[18,19]. As reported previously[20], the Δ*gntK* Δ*idnK* double mutant did not grow on D-gluconate as sole carbon source. As expected therefore, gluconate accumulation was observed when the *ΔpglΔgntKΔidnK* triple mutant was grown on glucose, with an excretion rate of 1.13 ± 0.04 mmol.(g_{CDW}·h)$^{-1}$. These results are consistent with the Pgl bypass topology described by Kupor and Fraenkel[14] (Figure 2).

An unforeseen consequence of gluconokinase deletion was that the Δ*pgl*Δ*gntK*Δ*idnK* triple mutant had a much slower growth rate than the Δ*pgl* strain (0.29 ± 0.01 h^{-1} *vs.* 0.43 ± 0.01 h^{-1}). This highlights

the importance of metabolic activity in the bypass pathway to sustain growth. To investigate this further, we quantified the metabolic flux through the extracellular bypass using ^{13}C metabolic flux analysis. Since the bypass pathway and the non-enzymatic hydrolysis of δ-6PGL operate in parallel without carbon scrambling, their relative contributions to the oxPPP flux cannot be determined using stationary ^{13}C labelled experiments alone. We therefore investigated the contributions of both routes in the Δ*pgl* strain using stationary and non-stationary metabolic flux analyses.

Deletion of *pgl* barely modifies the contribution of the oxidative branch of the PPP to glucose metabolism

We first quantified the distribution of glucose-6-phosphate between the Embden-Meyerhof-Parnas (EMP) pathway and the oxPPP in the Δ*pgl* strain and the WT strain (as control) grown on minimal M9 medium supplemented with [1-^{13}C]-glucose as sole carbon source. Metabolic fluxes were inferred from quantitative measurements of ^{13}C incorporation into alanine *via* pyruvate (Figure 3). In keeping with previous results[6,21], 17 ± 1 % of glucose was channelled through the oxPPP in the WT strain. In the Δ*pgl* strain, the oxPPP accounted for 15 ± 1 % of glucose uptake, a similar contribution as in the WT strain. This suggests that the absence of Pgl does not lead to a rewiring of central metabolic fluxes, in contrast to what has been observed in the absence of glucose-6-phosphate dehydrogenase, the first enzyme in the oxPPP[6,7]. In the *Δpgl* strain, the metabolic flux through the oxPPP must therefore be maintained by the Pgl bypass and/or by non-enzymatic intracellular hydrolysis of δ-6PGL.

In the absence of Pgl, oxPPP flux passes exclusively though the Pgl bypass

To quantify the contributions of the extracellular bypass and of intracellular non-enzymatic δ-6PGL hydrolysis to oxPPP flux, we performed a non-stationary carbon labelling experiment wherein ^{13}C labelled glucose was added at the mid-exponential phase to *E. coli* Δ*pgl* growing on unlabelled glucose (Figure 4a and 4c). We used [2-^{13}C]-glucose because the NMR signals corresponding to [2-^{13}C]-glucose and [2-^{13}C]-gluconolactones formed from [2-^{13}C]-glucose, are well resolved in 1D,^{1}H NMR spectra, allowing accurate quantification of the total concentrations of unlabelled and labelled gluconolactone

(Figure 4b) over time, sampling the culture medium every 30 min after ^{13}C labelled glucose was added. Metabolic fluxes were calculated using a differential equation model of the metabolic network shown in Figure 4d. The flux through the oxPPP and the constant rate of gluconolactone hydrolysis were set to their experimentally determined values (Figure 1d and 3c). The metabolic fluxes were then obtained by fitting them to the time-course concentrations of biomass, (unlabelled and labelled) glucose and (total and ^{13}C-labelled) gluconolactone. Sensitivity analysis confirmed that the system was identifiable based on the available data, meaning that all fluxes were determined with high precision (relative standard deviation below 5 % in each of the three independent biological replicates).

The estimated glucose uptake rates and the growth rates were consistent with data obtained from unlabelled experiments (Table 1). The intracellular branch accounts for a negligible proportion of oxPPP flux (< 1 ± 1 % of glucose uptake), which is fully channelled through the extracellular bypass (99 ± 1 %). The bypass carries a flux of 1.07 ± 0.08 mmol·(g_{CDW}·h)$^{-1}$ which is similar to the flux through the canonical oxPPP in the WT strain and much higher than the gluconolactone accumulation flux in unlabelled experiments (0.17 mmol·(g_{CDW}.h)$^{-1}$, Table 1). Overall, these results demonstrate the absence of intracellular flux through the canonical oxPPP under these circumstances, and reveal the key contribution of the extracellular Pgl bypass to R5P biosynthesis in the Δ*pgl* strain. These results also explain the severe growth restriction observed when the Pgl bypass is blocked by the deletion of gluconokinases.

DISCUSSION

To our knowledge this work is the first time the metabolic activity of the Pgl bypass has been quantified, despite its discovery in *E. coli* more than fifty years ago[14]. Our NMR results confirm the bypass topology proposed by Kupor and Fraenkel, although the 6PGL dephosphorylation and (P-)gluconolactone secretion steps remain to be elucidated. Metabolite phosphatases are generally cytosolic, although some have been shown to be periplasmic, notably those involved in nucleotide salvage[22]. If 6PGL is secreted in its phosphorylated form, it should be found in the culture medium

based on the spontaneous hydrolysis rate estimated in this work. Since 6PGL was not detected, this suggests it is dephosphorylated intracellularly and that it is the resulting gluconolactone that is then secreted. Nevertheless, further studies are required to identify the genes involved in dephosphorylation and secretion of gluconolactones and to unequivocally resolve the first two steps of the Pgl bypass.

Because of this bypass, absence of Pgl leads to substantial gluconolactone excretion – about 17% of the total carbon flux entering the cell. This process, which resembles directed overflow mechanism[23], prevents 6PGL intracellular accumulation, avoiding covalent modifications of proteins[24] and other nucleophiles[10] in the presence of these highly reactive electrophiles. Gluconolactone excretion may therefore be a cleansing mechanism that avoids the formation of toxic metabolites, the function generally ascribed to Pgl[12]. The Pgl bypass may therefore have arisen fortuitously because the unstable gluconolactones excreted into the environment spontaneously hydrolyse into gluconate, one of *E. coli*'s preferred carbon sources[25].

The Pgl bypass produces pentose-phosphates and NAPDH from G6P with the same stoichiometry as the canonical oxPPP. However, this extracellular metabolic route has a significant energetic cost for the cell. First, one extra mole of ATP is required for the phosphorylation of gluconate by gluconokinases (GntK and IdnK). Second, gluconate import is mediated by proton symport systems driven by the proton motive force (with a stoichiometry of one proton per gluconate[26,27]), thereby consuming protons that could otherwise be used by ATP synthases for ATP production. Assuming a maximal H^+/ATP ratio of 4[28], the total energetic cost of the Pgl bypass is 1.25 ATP equivalents per molecule of glucose entering the oxPPP, corresponding to an extra ATP demand of 1.33 $mmol \cdot [g_{CDW} \cdot h]^{-1}$. In other words, roughly 20% of the energy used by the cell for glucose uptake and subsequent phosphorylation by the PTS system is wasted in the Pgl bypass. Furthermore, because gluconolactone hydrolysis occurs non-enzymatically outside the cell, it escapes direct metabolic control and the gluconolactone and gluconate are potentially accessible to other cells competing for carbon sources. An illustrative

example of this kind of cross-feeding is the recovery of normal growth in Δ*zwf*Δ*pgi* *E. coli* in the presence of Δ*pgl* mutants, likely because the gluconolactone or gluconate released by the latter feed the oxPPP of the Δ*zwf*Δ*pgi* cells[15]. The downsides of this extracellular bypass are therefore that it is more energetically expensive, partially beyond metabolic regulation and subject to hijack by competing cells.

Two oxPPP topologies must therefore be considered in metabolic flux analyses depending on whether Pgl is present (the canonical oxPPP) or absent (with Pgl bypass). The latter configuration is generally ignored however[7,29], particularly in analyses of *E. coli* BL21[30,31], which is widely used in biotechnological applications, notably for heterologous protein production[32]. *E. coli* BL21 and derived strains lack the *pgl* gene and there is evidence of Pgl bypass activity in this strain[33].

Our results show that metabolic activity in the Pgl bypass oxPPP is similar to that of the canonical oxPPP in the WT strain. As observed previously though[7,14,15], the Δ*pgl* mutant grows about 30% slower than the WT. The growth rate is reduced even further if gluconate utilisation is also blocked (down to about 50% of the WT's growth rate), highlighting the metabolic contribution of the Pgl bypass. Finally, of the three enzymes involved in the oxPPP (Pgl, G6P dehydrogenase, and 6PGNT dehydrogenase, the latter two being encoded by *zwf* and *gnd* respectively), Pgl is the only one whose absence is associated with a noticeable growth defect. In particular, the silent growth phenotype of the Δ*zwf* mutant demonstrates that flux in the oxPPP is not absolutely required for bacterial growth on glucose. Deletion of *zwf* leads to a global reorganization of metabolic fluxes through *E. coli*'s central metabolism to compensate for the absence of flux in the oxPPP while providing the required precursors and energy for anabolism[6,34,35]. In contrast, *pgl* deletion leads to a local rearrangement of carbon fluxes that fails to support optimal growth. Furthermore, in spite of the secretion mechanism described in this study, absence of Pgl must nevertheless lead to intracellular accumulation of δ-6PGL, Pgl's substrate, and γ-6PGL, which forms faster by isomerization of δ-6PGL than δ-6PGL spontaneously hydrolyses to 6PGNT[11]. Indeed, δ-6PGL accumulation has been observed in *E. coli* BL21 growing on glucose[33]. The

accumulation of these reactive compounds may be detrimental to cells. The growth defect of the Δ*pgl* mutant can therefore be explained by the energy cost of the Pgl bypass and/or intracellular accumulation of toxic intermediates.

Pgl is often described as predominantly a house-cleaning enzyme, preventing the formation of undesirable by-products[9,12]. According to this view, oxPPP flux should mainly be maintained by non-enzymatic hydrolysis of 6PGL into 6PGNT[7,12,14]. Our results shown on the contrary that the contribution of non-enzymatic δ-6PGL hydrolysis to the canonical oxPPP in the absence of Pgl is negligible, a situation (absence of Pgl) that should promote non-enzymatic hydrolysis of δ-6PGL, since the intracellular concentration of the latter is increased, as mentioned above[33]. We can therefore assume that non-enzymatic hydrolysis of δ-6PGL is also negligible when Pgl is present (*i.e.* in the WT strain), meaning that the Pgl's catalytic activity is crucial for 6PG formation. Our results therefore suggest that Pgl's catalytic role is crucial for the efficient functioning of the central metabolic network. While Pgl does also help prevent intracellular accumulation of 6PGLs, our results suggest that this role is mediated by an additional process involving the excretion of these compounds from the cell.

In summary, our comprehensive functional analysis of a knock-out mutant in *E. coli*'s central metabolism confirms the existence of a long described compensatory mechanisms and reveals fundamental gaps in our current understanding of an enzyme operating in parallel to a non-enzymatic reaction. Because the reaction catalysed by Pgl can occur spontaneously, the role of Pgl in metabolism has remained unclear. Our results indicate that Pgl's catalysis of 6PGL hydrolysis into 6PGNT is crucial to maintain the required flux through the oxPPP in an energy-efficient manner.

METHODS

Strains and media.

Escherichia coli K-12 BW25113 was selected as the experimental model (wild-type strain) for this study. *E. coli* BW25113 *Δpgl* was constructed from a Δ*pgl* strain in the Keio collection[36], with kanamycin cassette removal with a pCP20 plasmid encoding FLP recombinase[37]. The deletion mutant *ΔpglΔgnt* was obtained via a one-step disruption protocol[38], and the triple deletion mutant *ΔpglΔgntΔIdnK* similarly from the double *ΔpglΔgnt* mutant. To confirm the mutations, polymerase chain reaction (PCR) was used to amplify fragments containing the modified sequences. The lengths of the amplified fragments were tested by agarose gel electrophoresis and compared with those of the previous mutant strain. The complemented strain (*Δpgl::pgl*) was obtained by transformation of the *Δpg*l strain by a pZA23::*pgl* plasmid carrying the *pgl* gene under the control of the pLac promoter. The *pgl* gene was amplified from the *E. coli* BW25113 WT strain by PCR and inserted in pZA23 plasmid using the In-Fusion® HD Cloning Plus CE Kit (Takara).

All *E. coli* strains were grown in M9-based minimal synthetic medium as described in[6], complemented with 15 mM glucose. Cultures (50 mL) were performed in triplicate in baffled shake flasks at 37 °C and 200 rpm. Growth was monitored by measuring the optical density at 600 nm (OD_{600}) using a Genesys 6 spectrophotometer (Thermo, USA), and a correlation factor of 0.37 ($g_{CDW}\cdot L^{-1})\cdot OD_{600}^{-1}$ was used to calculate biomass concentration.

NMR analysis

NMR spectra were recorded on a Bruker Avance III HD 800 MHz spectrometer equipped with a 5-mm quadruple-resonance QCI-P (H/P-C/N/D) cryogenically cooled probe head. D_2O (10 vol.%) was added to the samples for field/frequency locking and 1 mM TSP-d4 (dissolved in D_2O) was added as an internal standard for frequency calibration and concentration measurements. Spectra were recorded and processed using Bruker TopSpin 3.2. 1D ^1H NMR spectra were acquired using the zgpr30 sequence at 280 K with 32 or 64 scans, 64k points, an acquisition time of 2 s, and an recycle delay of 8 s.

Extracellular metabolite concentration measurements and calculation of extracellular fluxes.

Metabolite concentrations (glucose, acetate, gluconate (GNT)) were quantified by 1D ^{1}H NMR from the supernatant obtained by centrifugation (12,000 g, 3 min) of culture broth. The 1D ^{1}H NMR data were acquired as described above (64 scans). For samples containing gluconolactone (GL), the metabolites (including glucose, gluconate and gluconolactone) were quantified immediately after filtration (0.2 µm, polyethersulfone membrane) of 500 µL of culture. The filtrate was kept on ice and rapidly analysed by NMR as described above (32 scans).

Extracellular fluxes (*i.e.* glucose uptake, GNT accumulation and growth rates) were determined from the time course concentrations of biomass, substrates, and products using PhysioFit v2.0.4[39](https://github.com/MetaSys-LISBP/PhysioFit).

Stationary ^{13}C- labelling experiments

After preculture on LB, strains were grown in 50 ml M9 minimal synthetic medium complemented with 15 mM [1-^{13}C] glucose in baffled shake flasks at 37 °C and 200 rpm. At OD 1.2, cells were harvested by centrifugation (5 min at 10,000 g) and the pellet was resuspended in 1.250 ml of Milli-Q H_2O. The suspension (250 µl) was mixed with 250 µl of HCl 12N and hydrolysed at 110 °C for 18 h. HCl was evaporated using a vacuum concentrator, the pellet was washed twice with Milli-Q H_2O and resuspended in 100 µl H_20. This sample was diluted 100 times for analysis. The carbon isotopologue distribution of alanine was measured in three independent biological replicates, as detailed in[40].

^{13}C-Pulse experiments

E. coli BW25113 *Δpgl* was grown in 50 ml M9 minimal synthetic medium complemented with 15 mM glucose in a baffled shake flask at 37 °C and 200 rpm. At OD 1.2, [2-^{13}C] glucose was added to the culture medium to obtain approximately 50 % of ^{13}C-labelled glucose. Growth was monitored using OD_{600} measurements as described above. Extracellular compounds were quantified directly by NMR as described above.

298 **Kinetics of phosphogluconolactone and gluconolactone spontaneous hydrolysis**

299 *Real time monitoring of gluconolactone (GL) degradation*. δ-Gluconolactone (δ-GL) degradation was
300 monitored by ^{1}H NMR using a pseudo-2D pulse program (noesyphpr) at 310K. A 3 mM δ-GL (Sigma-
301 Aldrich) solution was prepared in M9-based minimal synthetic medium. Acquisitions were started after
302 rapid homogenisation and temperature stabilisation, and spectra were recorded every 65 s with 8
303 scans each (acquisition time, 3 s; recycle delay, 5 s) for a total of 120 time points. δ-GL degradation at
304 280 K was monitored using the same procedure and a freshly prepared δ-GL solution.

305 *Real time monitoring of 6-phosphogluconolactone (6PGL) degradation*. 6PGL was produced
306 enzymatically from glucose-6-phosphate (G6P) using commercial *L. mesenteroides* $NADP^{+}$ dependent
307 G6P-dehydrogenase (G6PDH) expressed in *E. coli* (Sigma-Aldrich). The reaction mix consisted of 5 mM
308 G6P, 5 mM $NADP^{+}$, 12 mM $MgCl_2$, 100 mM phosphate buffer (at pH = 7.2) and 1 mM TSP-d4[6]. ^{1}H and
309 ^{31}P 1D NMR spectra of the mix were recorded using the zgpr30 sequence with 16 scans and the zg
310 sequence with 64 scans, respectively. One enzyme unit of G6PDH was then added to the NMR tube
311 and the production and hydrolysis of 6PGL were monitored at 310 K using dual reception (^{1}H and ^{31}P)
312 pseudo-2D spectra (2DDR zggpw5)[41]. Spectra were recorded every 115 s with 64 scans each for a total
313 of 64 time points (^{1}H acquisition time, 0.7 s; recycle delay; ^{31}P acquisition time 0.6 s, recycle delay, 1
314 s). The concentrations of G6P, 6PGL and 6PGNT were determined from the rows of the pseudo-2D ^{31}P
315 spectra.

316 *Calculation of degradation constants***.** The degradation constants of GL and 6PGL were determined by
317 fitting their time-course concentrations assuming a first-order process using COPASI[42] (v4.27), as
318 detailed in[17].

319 **Relative contributions of glycolysis and the oxPPP**

320 The contributions of the oxPPP and Emben-Meyerhof-Parnas (EMP) pathway to glucose metabolism
321 were estimated by quantifying alanine isotopologues. [1-^{13}C] glucose metabolised through the EMP
322 pathway forms unlabelled and [1-^{13}C] pyruvate in equal proportions, while C_1-decarboxylation of

323 glucose through the oxPPP only produces unlabelled pyruvate. The contributions of the oxPPP and the
324 EMP pathway were thus estimated from the fraction of the M1 isotopologue of alanine, using the
325 following algebraic equations[21]:

326 $$Glycolysis = 2 \times Ala_{M1}$$

327 $$PPP = 2 \times (0.5 - Ala_{M1})$$

328

329 **Dynamic ^{13}C-flux model of glucose metabolism to quantify the contribution of the Pgl bypass**

330 To quantify the contributions of the canonical oxPPP and of the Pgl bypass to ribose-5-phosphate
331 biosynthesis, we constructed a dynamic ^{13}C-flux model of glucose metabolism following the formalism
332 detailed in[43]. The model contains 21 reactions, 25 species, and 2 compartments (the environment and
333 the cell), and represents five processes: i) growth, ii) glucose uptake and phosphorylation into G6P,
334 utilisation of G6P through iii) the EMP pathway and iv) the intracellular branch of the oxPPP, and v) the
335 extracellular Pgl bypass (Figure 4).

336 The differential equations, which balance the concentrations of extracellular compounds (biomass,
337 glucose, gluconolactone and gluconate) and intracellular compounds (G6P, glyceraldehyde-3-
338 phosphate, 6PGL, 6PGNT and pyruvate), were completed with isotopic equations for parameter
339 estimation. As detailed in [43,44], we considered all reactions (except biomass synthesis) separately for
340 unlabelled and labelled reactants. Fluxes were assumed to be constant over time, in line with the
341 metabolic steady-state assumption, except for the gluconolactone hydrolysis flux which was modelled
342 using the mass action law to represent first-order degradation kinetics[17], in keeping with the abiotic
343 hydrolysis of gluconolactone into gluconate (see Results).

344 The final model has 8 free parameters in total (Supplementary 2). The contribution of the oxPPP to
345 glucose metabolism (*i.e.* the sum of the flux through the intra- and extracellular branches of the oxPPP)
346 and the gluconolactone (abiotic) hydrolysis rate were fixed at the experimental values determined in
347 this study, as detailed in the Results section. The remaining parameters (p) were estimated by fitting

to the experimentally determined concentration dynamics of biomass and unlabelled and labelled glucose and gluconolactone, by minimising the objective function *f* defined as the weighted sum of squared errors:

$$f(p) = \sum_i \left(\frac{x_i - y_i(p)}{\sigma_i} \right)^2$$

where x_i is the experimental value of data point *i*, with an experimental standard deviation σ_i, and $y_i(p)$ is the corresponding simulated value. The objective function *f* was minimised using the particle swarm optimisation algorithm (2,000 iterations with a swarm size of 50). The experimental and fitted data of one biological replicate are shown in Figure 4, and the data for all replicates are provided in the Supplementary 2.

The model was constructed and analysed using COPASI[42] (v4.27) and is provided in SBML and COPASI formats in the Supplementary 2 and at https://github.com/MetaSys-LISBP/GL_GNT_bypass. The model has also been deposited in the Biomodels database (https://www.ebi.ac.uk/biomodels)[45] with the identifier MODEL2310250001 to ensure reproducibility and reusability.

Supplementary Material

Supplementary material 1 : Figure 1, Figure 2, figure 3 et Figure 4

Supplementary material 2: Model documentation

Acknowledgements

This study was funded by the Agence Nationale de la Recherche, grant number ANR-19-CE44-0005 (PerioMet).

The authors thank MetaToul (Metabolomics & Fluxomics Facilities, Toulouse, France, www.metatoul.fr) and its staff for technical support and access to the NMR facility. MetaToul is part of the French National Infrastructure for Metabolomics and Fluxomics (www.metabohub.fr), funded by the ANR (MetaboHUB-ANR-11-INBS-0010).

371

372 **REFERENCES (50 max.)**

373 1. Edwards, J. S. & Palsson, B. O. Robustness analysis of the Escherichia coli metabolic network.
374 *Biotechnol Prog* 16, 927–939 (2000).
375 2. Nakahigashi, K. *et al.* Systematic phenome analysis of Escherichia coli multiple-knockout mutants
376 reveals hidden reactions in central carbon metabolism. *Mol Syst Biol* 5, 306 (2009).
377 3. Emmerling, M. *et al.* Metabolic flux responses to pyruvate kinase knockout in Escherichia coli. *J*
378 *Bacteriol* 184, 152–164 (2002).
379 4. Jiao, Z., Baba, T., Mori, H. & Shimizu, K. Analysis of metabolic and physiological responses to gnd
380 knockout in Escherichia coli by using C-13 tracer experiment and enzyme activity measurement.
381 *FEMS Microbiol Lett* 220, 295–301 (2003).
382 5. Siddiquee, K. A. Z., Arauzo-Bravo, M. J. & Shimizu, K. Effect of a pyruvate kinase (pykF-gene)
383 knockout mutation on the control of gene expression and metabolic fluxes in Escherichia coli.
384 *FEMS Microbiology Letters* 235, 25–33 (2004).
385 6. Nicolas, C. *et al.* Response of the central metabolism of Escherichia coli to modified expression of
386 the gene encoding the glucose-6-phosphate dehydrogenase. *FEBS Lett.* 581, 3771–3776 (2007).
387 7. Long, C. P. & Antoniewicz, M. R. Metabolic flux responses to deletion of 20 core enzymes reveal
388 flexibility and limits of E. coli metabolism. *Metabolic Engineering* 55, 249–257 (2019).
389 8. Sorokina, M., Stam, M., Médigue, C., Lespinet, O. & Vallenet, D. Profiling the orphan enzymes.
390 *Biology Direct* 9, 10 (2014).
391 9. Keller, M. A., Piedrafita, G. & Ralser, M. The widespread role of non-enzymatic reactions in cellular
392 metabolism. *Current Opinion in Biotechnology* 34, 153–161 (2015).
393 10. Rakitzis, E. T. & Papandreou, P. Reactivity of 6-phosphogluconolactone with hydroxylamine: The
394 possible involvement of glucose-6-phosphate dehydrogenase in endogenous glycation reactions.
395 *Chemico-Biological Interactions* 113, 205–216 (1998).
396 11. Miclet, E. *et al.* NMR spectroscopic analysis of the first two steps of the pentose-phosphate
397 pathway elucidates the role of 6-phosphogluconolactonase. *J Biol Chem* 276, 34840–34846 (2001).

12. Galperin, M. Y., Moroz, O. V., Wilson, K. S. & Murzin, A. G. House cleaning, a part of good housekeeping. *Molecular Microbiology* 59, 5–19 (2006).
13. Kupor, S. R. & Fraenkel, D. G. 6-phosphogluconolactonase mutants of Escherichia coli and a maltose blue gene. *J Bacteriol* 100, 1296–1301 (1969).
14. Kupor, S. R. & Fraenkel, D. G. Glucose Metabolism in 6-Phosphogluconolactonase Mutants of Escherichia coli. *Journal of Biological Chemistry* 247, 1904–1910 (1972).
15. Thomason, L. C., Court, D. L., Datta, A. R., Khanna, R. & Rosner, J. L. Identification of the Escherichia coli K-12 ybhE gene as pgl, encoding 6-phosphogluconolactonase. *J Bacteriol* 186, 8248–8253 (2004).
16. Enjalbert, B., Letisse, F. & Portais, J.-C. Physiological and Molecular Timing of the Glucose to Acetate Transition in Escherichia coli. *Metabolites* 3, 820–837 (2013).
17. Peiro, C. *et al.* Chemical and Metabolic Controls on Dihydroxyacetone Metabolism Lead to Suboptimal Growth of Escherichia coli. *Appl Environ Microbiol* 85, (2019).
18. Tong, S., Porco, A., Isturiz, T. & Conway, T. Cloning and molecular genetic characterization of the Escherichia coli gntR, gntK, and gntU genes of GntI, the main system for gluconate metabolism. *Journal of Bacteriology* 178, 3260–3269 (1996).
19. Istúriz, T., Palmero, E. & Vitelli-Flores, J. Mutations affecting gluconate catabolism in Escherichia coli. Genetic mapping of the locus for the thermosensitive gluconokinase. *J Gen Microbiol* 132, 3209–3219 (1986).
20. Bausch, C., Ramsey, M. & Conway, T. Transcriptional Organization and Regulation of the l-Idonic Acid Pathway (GntII System) in Escherichia coli. *Journal of Bacteriology* 186, 1388–1397 (2004).
21. Millard, P., Cahoreau, E., Heuillet, M., Portais, J.-C. & Lippens, G. 15N-NMR-Based Approach for Amino Acids-Based 13C-Metabolic Flux Analysis of Metabolism. *Anal. Chem.* 89, 2101–2106 (2017).
22. Neidhart, F. C. & Curtiss, R. Escherichia coli and Salmonella—Cellular and molecular biology. in *Escherichia coli and Salmonella—Cellular and molecular biology* (SM Press, 1996).

23. Reaves, M. L., Young, B. D., Hosios, A. M., Xu, Y.-F. & Rabinowitz, J. D. Pyrimidine homeostasis is accomplished by directed overflow metabolism. *Nature* 500, 237–241 (2013).

24. Aon, J. C. *et al.* Suppressing Posttranslational Gluconoylation of Heterologous Proteins by Metabolic Engineering of *Escherichia coli*. *Appl Environ Microbiol* 74, 950–958 (2008).

25. Chang, D.-E. *et al.* Carbon nutrition of Escherichia coli in the mouse intestine. *Proc Natl Acad Sci U S A* 101, 7427–7432 (2004).

26. Neidhart, F. C., Ingraham, J. L. & Schaechter, M. *Physiology of the bacterial cell: a molecular approach.* (1990).

27. Robin, A. & Kepes, A. The mechanism of maintenance of electroneutrality during the transport of gluconate by E. coli. *FEBS Letters* 36, 133–136 (1973).

28. Steigmiller, S., Turina, P. & Gräber, P. The thermodynamic H+/ATP ratios of the H+-ATPsynthases from chloroplasts and Escherichia coli. *Proc Natl Acad Sci U S A* 105, 3745–3750 (2008).

29. Ishii, N. *et al.* Multiple High-Throughput Analyses Monitor the Response of E. coli to Perturbations. *Science* 316, 593–597 (2007).

30. Theodosiou, E., Frick, O., Bühler, B. & Schmid, A. Metabolic network capacity of Escherichia coli for Krebs cycle-dependent proline hydroxylation. *Microbial Cell Factories* 14, 108 (2015).

31. Kim, H., Kim, S. & Yoon, S. H. Metabolic network reconstruction and phenome analysis of the industrial microbe, Escherichia coli BL21(DE3). *PLOS ONE* 13, e0204375 (2018).

32. Terpe, K. Overview of bacterial expression systems for heterologous protein production: from molecular and biochemical fundamentals to commercial systems. *Appl Microbiol Biotechnol* 72, 211–222 (2006).

33. Meier, S., Jensen, P. R. & Duus, J. Ø. Direct observation of metabolic differences in living Escherichia coli strains K-12 and BL21. *Chembiochem* 13, 308–310 (2012).

34. Fischer, E. & Sauer, U. Metabolic flux profiling of Escherichia coli mutants in central carbon metabolism using GC-MS. *European Journal of Biochemistry* 270, 880–891 (2003).

449 35. Zhao, J., Baba, T., Mori, H. & Shimizu, K. Effect of zwf gene knockout on the metabolism of
450 Escherichia coli grown on glucose or acetate. *Metab Eng* 6, 164–174 (2004).
451 36. Baba, T. *et al.* Construction of Escherichia coli K-12 in-frame, single-gene knockout mutants: the
452 Keio collection. *Mol. Syst. Biol.* 2, 2006.0008 (2006).
453 37. Cherepanov, P. P. & Wackernagel, W. Gene disruption in Escherichia coli: TcR and KmR cassettes
454 with the option of Flp-catalyzed excision of the antibiotic-resistance determinant. *Gene* 158, 9–14
455 (1995).
456 38. Datsenko, K. A. & Wanner, B. L. One-step inactivation of chromosomal genes in Escherichia coli K-
457 12 using PCR products. *Proc Natl Acad Sci U S A* 97, 6640–6645 (2000).
458 39. Grégam, L. L. *et al.* PhysioFit: a software to quantify cell growth parameters and extracellular
459 fluxes. 2023.10.12.561695 Preprint at https://doi.org/10.1101/2023.10.12.561695 (2023).
460 40. Heuillet, M. *et al.* Methodology for the Validation of Isotopic Analyses by Mass Spectrometry in
461 Stable-Isotope Labeling Experiments. *Anal. Chem.* 90, 1852–1860 (2018).
462 41. Cox, N. *et al.* Integrated pH Measurement during Reaction Monitoring with Dual-Reception 1H-
463 31P NMR Spectroscopy. *Anal Chem* 91, 3959–3963 (2019).
464 42. Hoops, S. *et al.* COPASI--a COmplex PAthway SImulator. *Bioinformatics* 22, 3067–3074 (2006).
465 43. Millard, P., Portais, J.-C. & Mendes, P. Impact of kinetic isotope effects in isotopic studies of
466 metabolic systems. *BMC Syst Biol* 9, 64 (2015).
467 44. Enjalbert, B., Millard, P., Dinclaux, M., Portais, J.-C. & Létisse, F. Acetate fluxes in Escherichia coli
468 are determined by the thermodynamic control of the Pta-AckA pathway. *Sci Rep* 7, 42135 (2017).
469 45. Chelliah, V. *et al.* BioModels: ten-year anniversary. *Nucleic Acids Res* 43, D542-548 (2015).
470 46. Le Novère, N. *et al.* The Systems Biology Graphical Notation. *Nat Biotechnol* 27, 735–741 (2009).
471

472

TABLES

Table 1: Growth parameters of the different *E. coli* K12 BW25113 strains grown in minimal media with 15mM glucose.

The growth of the *E. coli* BW25113 *Δpgl* strain was compared to the WT strain's and that of the complemented strain, Δ*pgl*::pZA23*pgl*, obtained by transformation of the *Δpgl* strain with pZA23::pgl plasmid and of the Δ*pgl*::pZA23 strain with an empty plasmid. μ_{max}, specific growth rate; q_{Glc}, glucose uptake rate; q_{Ac}, net acetate production rate; q_{Gnt}, gluconate accumulation rate. Results are the mean ± SD of three biologically independent samples.

Parameters	WT	Δ*pgl*	Δ*pgl*::pZA23*pgl*	Δ*pgl*::pZA23
μ_{max} (h^{-1})	0.61 ± 0.01	0.43 ± 0.01	0.57 ± 0.01	0.41 ± 0.01
q_{Glc} (mmol · [g_{CDW} · h]$^{-1}$)	7.77 ± 0.17	8.52 ± 0.39	10.11 ± 0.83	7.60 ± 0.08
q_{Ace} (mmol · [g_{CDW} · h]$^{-1}$)	2.37 ± 0.15	4.56 ± 0.16	7.60 ± 0.31	3.95 ± 0.16
q_{Gnt} (mmol · [g_{CDW} · h]$^{-1}$)	0	0.17 ± 0.01	0	0.14 ± 0.02

485 **FIGURES (6 max. in the main text)**

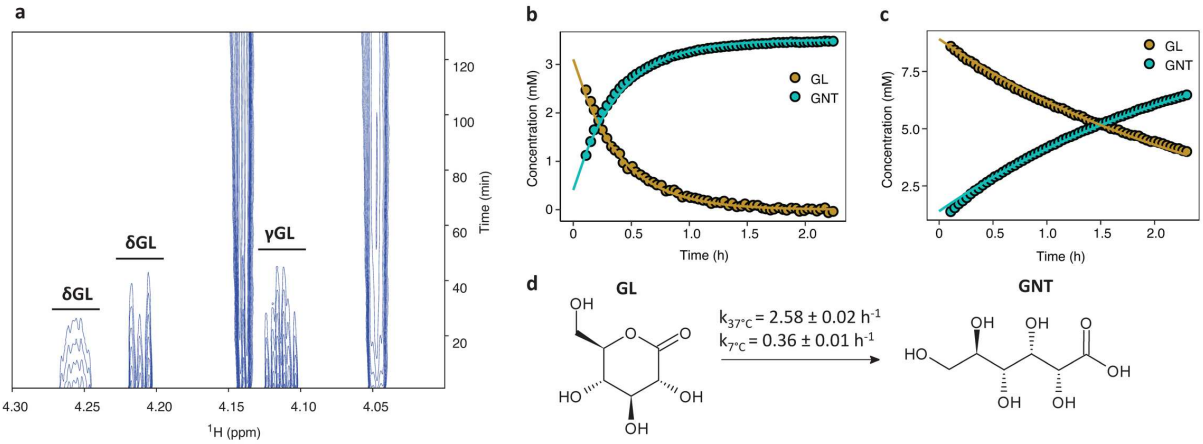

486

487 **Figure 1. Gluconolactone spontaneous hydrolysis**. **a**. Pseudo-2D ^{1}H spectra at 37°C, pH7.2 in M9
488 synthetic minimal media of spontaneous gluconolactone hydrolysis. T0 corresponds to the beginning
489 of NMR acquisition (= 6 min 35 s after gluconolactone addition). **b,c**. GL and GNT concentrations
490 extracted from pseudo-2D spectra (dots) and fitted by COPASI model (lines) at 37 °C (**b**) and 7 °C (**c**). **d.**
491 Reaction scheme for the spontaneous hydrolysis of gluconolactone (GL) into gluconic acid (GNT) with
492 the degradation constant obtained at 37 °C and 7 °C.

493

494

Figure 2:

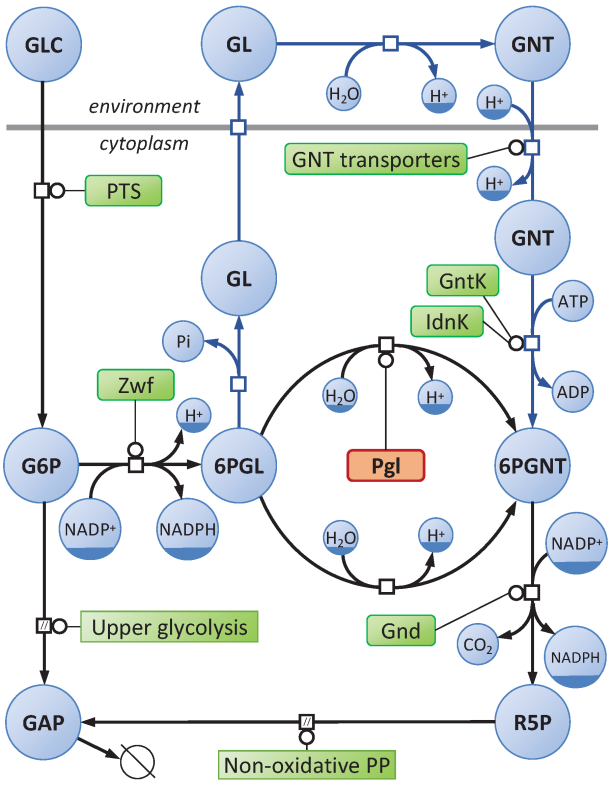

Figure 2. Schematic representation of the Pgl bypass and of the oxidative branch of the pentose-phosphate (PP) pathway in *E. coli*, in Systems Biology Graphical Notation format[46] (http://sbgn.org.io). Circles represent metabolites and rounded rectangles represent enzymes. GLC, glucose; G6P, glucose-6-phosphate; GAP, glyceraldehyde-3-phosphate; 6PGL, 6-phosphogluconolactone; GL, gluconolactone; GNT, gluconate; 6PGNT, 6-phosphogluconate; R5P, ribulose-5-phosphate; PTS, Phosphoenolpyruvate:glucose phosphotransferase system; Zwf, glucose-6-phosphate dehydrogenase; GntK, gluconate kinase; IdnK, thermosensitive gluconate kinase; Gnd, 6-phosphogluconate.

506 **Figure 3**

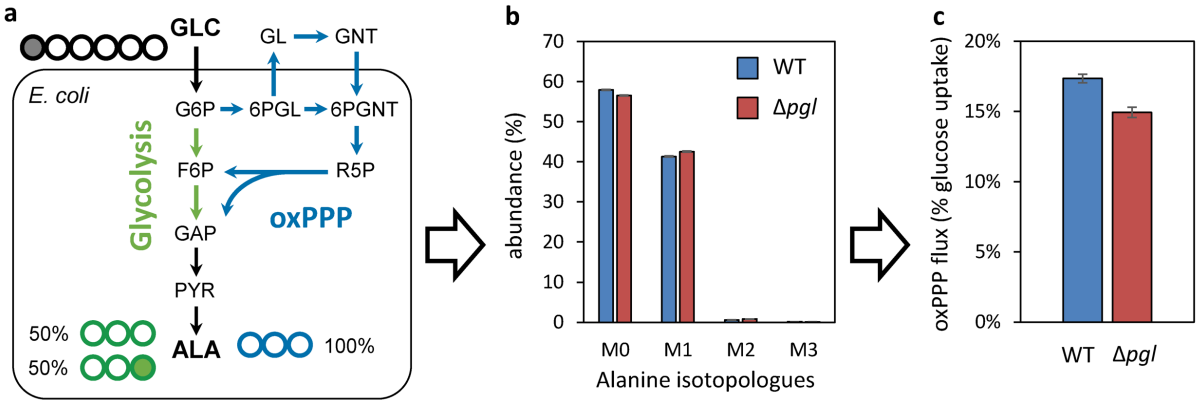

507

508 **Figure 3. Metabolic fluxes analysis of *E. coli* BW25113 wild-type (WT) and Δpgl strains.**

509 **a**. Cells were grown on 1-^{13}C-glucose, which can be metabolized through glycolysis (green pathway)
510 and the pentose phosphate pathway (blue pathway). Filled (empty) circles represent ^{13}C (^{12}C) atoms.
511 **b**. Isotopologue distribution of alanine measured by mass spectrometry. **c**. The partitioning of carbon
512 fluxes between glycolysis and the pentose phosphate pathway was quantified from the data shown in
513 panel b. The bars represent the mean of three biological replicates, and the error bars represent one
514 standard deviation.

515

516 **Figure 4 :**

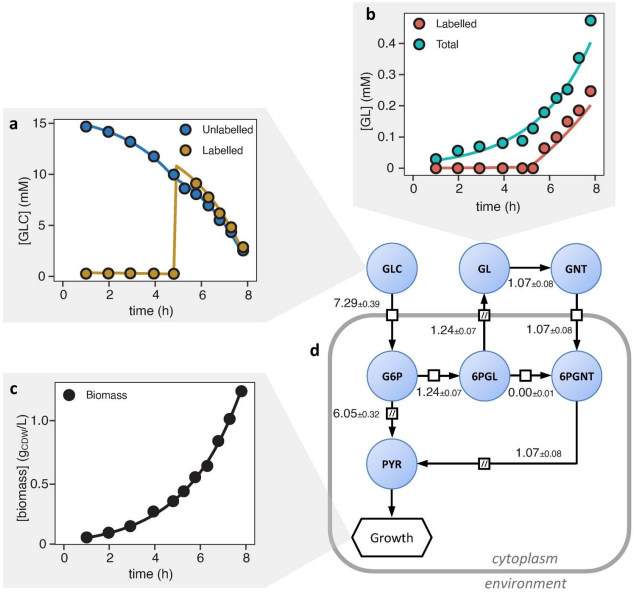

517

518 **Figure 4. Fluxes in the oxPPP of *E. coli* BW25113 Δ*pgl* quantified by non-stationary ^{13}C-metabolic flux**

519 **analysis.**

520 **a.** Concentrations of labelled and unlabelled glucose. [2-^{13}C]-glucose was added at mid-exponential

521 growth (approx. 5 h). **b.** Gluconolactone (labelled and total) concentrations. **c.** Growth of the Δ*pgl*

522 strain as a function of time. **d.** Metabolic network of the model used to calculate fluxes involved in the

523 Pgl bypass, with flux results (obtained from three independent biological replicates).

524

525